Fano resonances for localized intrinsic defects in finite-sized photonic crystals

S. Nojima,* M. Usuki, M. Yawata, and M. Nakahata
Department of Nanosystem Science, Graduate School of Nanobioscience, Yokohama City University, 22-2 Seto, Kanazawa, Yokohama, Kanagawa 236-0027, Japan
(Received 17 February 2012; published 18 June 2012)

Fano resonance spectroscopy (FRS) is used to investigate the photonic resonance properties of the defect states in two-dimensional finite-sized photonic crystals (PCs). This study examines the scattering cross-section spectra by changing the direction of the incident light continuously. The present FRS is applied to the intrinsic localized defect produced by displacing a single rod atom from its regular site, which creates one defect mode within the first gap and two defect modes within the second gap simultaneously. The present examination has made clear the correlation between the asymmetry of the scattering cross-section spectra—characterized by the so-called Fano q value—and the optical energy flows in the PC, in particular, that the optical incoming flux is maximized for $q^{-1} = 0$. This fact demonstrates the presence of the selective capturing of photons at the defect state in the incoming process of light; moreover, it can be recognized merely by knowledge of the q values. The Fano resonances have thus been successfully used to elucidate the resonance nature of the localized defect states in photonic crystals.

DOI: 10.1103/PhysRevA.85.063818 PACS number(s): 42.70.Qs, 78.67.Pt, 63.20.Pw, 42.60.Da

I. INTRODUCTION

The strong confinement of light in a small region is one of the primary concerns in recent nano- and microphotonics, because it finds a variety of applications in optical physics and engineering where it is exploited in low-threshold lasers [1], nonlinear optical devices [2], and cavity quantum electrodynamics devices [3]. This is entirely due to the anticipated enhancement of the interaction between light and matter systems, which is caused by the elongated dwelling time of light in that region. Extensive efforts have therefore been devoted to developing a cavity that can confine light efficiently—high-quality optical resonators using band-edge modes in photonic crystals (PCs) [4–10], circulating Bloch modes in a photonic atoll (a periodic closed chain array of microstructures) [11,12], whispering gallery modes (WGMs) in a single microstructure [13–17], and defect modes localized around a disorder in the PCs [18–21]. The last example (localized defect) is thought to be especially important because it provides very-high-quality factors (Q factors) and moreover, it has an advantage to occupy its part in the PC structure, which is one of the most promising substrates for the futuristic optical information processing technology.

The defects in PCs are often understood as the disorders which cause a significant modification of the optical density of states—the creation of isolated discrete states—in the photonic band gap when they are referred to particularly in a theoretical context. They have been investigated to date using a variety of theoretical methodologies: the Green's function method [22–25], the multiple scattering method [26–29], the supercells method [30,31], and the oscillating dipole-moment method [32,33]. These research results for the PC defects include those, e.g., for light localization [28,32,34], photon lifetimes or Q factors of the resonators [29,35–37], the local density of states [25], and the group-theoretic classifications of the modes [34]. Moreover, we should not forget that the PC defects can also be treated in terms of the Koster-Slater model [38] for the impurity states in semiconductors, as concisely reviewed by Ohtaka [39]. Despite so many reports published to date, however, it seems to the authors that few systematic investigations have been conducted from the physical point of view concerning the basic properties of these PC defects, e.g., the correlations among the defect formation processes, mode frequencies, photon lifetimes, and their resonance properties. Moreover, it seems to the authors that the interests concerning the disorders in PCs have been directed solely to the pursuit of defect structures that possess higher Q factors. Although the research in this direction is actually indispensable for the development of high-quality resonators, it appears to be somewhat devoid of the physical perspective for defects in the PCs.

Defects embedded in the PCs provide an ideal stage of research for the optical resonance phenomena. They create the isolated photonic states, i.e., states without the presence of any adjacent states in the photonic band gap, which would not require consideration of their interference with other adjacent states. The defect states in the finite-sized PCs can be regarded as the discrete states that are coupled to the continuous states outside the PC. This is exactly an analog to the electronic phenomena known as the autoionization for atoms [40], the predissociation for molecules [41], and the shape resonance (the quasibound state formation by a thin potential barrier) [42], and so on. The physics that lies behind all these phenomena could be epitomized as what is called the Fano resonance [43]. The Fano effects have been investigated in almost all fields of physics [44,45]; we can find much literature, especially in the research of semiconductor nanostructure physics [46–51]. The field of PC research is not an exception. Several reports have been published, which include the resonance of guided modes [52], bistability [53], photoluminescence [54], surface plasmon resonance [55], Mie and Bragg scatterings [56], and scattering by the nanocavity [57]. We feel, however, that most of these studies seem to focus on merely fitting the results with the asymmetric line shape—characterized by the famous Fano's q value—and do not examine the topic in more depth, e.g., to study the

*Author to whom correspondence should be addressed: nojima@yokohama-cu.ac.jp

physical meaning of the q values. In light of the above, we have investigated the relations between the line shape and other physical quantities for the isolated defect states and have reported some preliminary results in a previous letter [58].

In this paper, we first demonstrate the simultaneous formation of several modes in an intrinsic defect created by simply displacing a single lattice atom from its regular site. The mode positions and the photon lifetimes are shown to be tuned in a wide range by adjusting the atomic displacement. The latter part of this paper is devoted to the analysis of the scattering cross section of light scattered by PCs with the above intrinsic defects. By considering the analogy between the defect states in a PC and the electronic resonance states in an atom, we investigated the resonance structures of the defects in detail, in particular, focusing on the analysis of the asymmetric Fano-Beutler resonance profile in the angle-resolved scattering cross-section spectra. This paper presents the correlations between the so-called q value and the optical energy flux into the resonance centers. We believe that this kind of examination from a physical point of view will do much toward a better understanding of the behavior of light in the localized states, and will also contribute to the development of high-quality defect resonators using the PCs.

II. THEORY

A. Multiple scattering of light

The analytic multiple-scattering theory is used to evaluate the behavior of light for the PCs. Since the general theory is already described in detail in a previous report [6], here we only briefly outline the framework of the calculation. We consider a two-dimensional (2D) array consisting of a finite number N of cylindrical rods with radius a placed at arbitrary points in the background material (the air in this case). Since the primary purpose is to investigate the photonic modes in PCs, the rods are assumed to have no gain and loss. Here, we focus on the polarization for which the electric field is parallel to the rod axis (E polarization). Let us assume that a plane light wave is incident on the rod array. We focus on the light scattering by a specific rod, e.g., the nth rod. The light wave outside this rod is, of course, made up of the incident wave and the scattered wave. This incident wave on this specific nth rod must contain the waves scattered by all other rods ($n' = 1, 2, \ldots, N$, but $n' \neq n$) as well as the incident light wave sent from the outside of the PC. The waves scattered by other rods are expressed in terms of a variety of coordinates particular to the nth rods ($n' \neq n$). However, it is inconvenient to treat the wave field containing various different coordinates, so we transform the expression of these waves into a representation containing only the coordinates of the nth rod. The light wave (incident plus scattered waves) thus obtained outside the nth rod is connected to the solution inside this rod using the boundary conditions on the rod surface. The electric field of the total scattered wave $E^s(\mathbf{r})$ can be written as the sum of the scattered wave around each nth rod over all rods ($n = 1, 2, \ldots, N$):

$$E^s(\mathbf{r}) = \sum_{n=1}^{N} \sum_{l=-\infty}^{+\infty} b_{nl} H_l^{(1)}(kr_n) e^{il\theta_n} \equiv \mathbf{b} \cdot \boldsymbol{\varphi}(\mathbf{r}), \qquad (1)$$

using the l-partial wave expansion, where $H_l^{(1)}(x)$ is the Hankel function [59] of the first kind that has the asymptotic form of the outgoing wave. Here, $k = \omega/c$ is the wave number of light in the background (the air), and b_{nl} are the coefficients to be determined. The coordinates in Eq. (1) are defined as follows: $\mathbf{r}$ is the generic coordinate, and $\mathbf{r}_n \equiv (r_n, \theta_n) \equiv \mathbf{r} - \mathbf{R}_n$, where $\mathbf{R}_n$ indicates the location of the nth lattice point. Here, the second equality in Eq. (1) implies the inner product of vectors $\mathbf{b} = (b_{nl})$ and $\boldsymbol{\varphi}(\mathbf{r}) = [H_l^{(1)}(kr_n)e^{il\theta_n}]$. Here, vector $\mathbf{b}$ is calculated from the relation $\mathbf{b} = T^{-1}\mathbf{p}$, where $\mathbf{p}$ is a vector that is related to the wave number and the incident angle of the incident wave, and T is a matrix, the $(nl, n'l')$ elements of which are defined by

$$T_{nl,n'l'} = \delta_{nn'}\delta_{ll'} - (1 - \delta_{nn'}) e^{i(l'-l)\phi_{n'n}} H_{l-l'}^{(1)}(kR_{nn'}) s_l, \qquad (2)$$

where δ is Kronecker's delta, $R_{nn'}$ is the distance between the centers of the nth and n'th rods, and $\phi_{n'n}$ is the angle that indicates the direction of the n'th rod center as viewed from the nth rod center. Here, s_l is a parameter related to the boundary conditions at the rod surface: see the Appendix in the previous report [6] for its details. The scattered-wave field is thus uniquely determined, provided that we are given the information of the PC structure and the incident wave.

B. Photonic modes and lifetimes

Let us consider the analogy between the electronic scattering by an atom and the photonic scattering by a finite-sized PC. First, we assume that several resonance states are formed in an atom, e.g., by the thin potential barrier surrounding it. The wave function of an electron has a large value inside the atom, and it decays exponentially into the barrier and continues to the oscillating continuous states outside (the tunneling effect). This state can be regarded as a quasidiscrete state that resonates with the continuum and therefore has an energy spectrum of a finite width. The scattering of an electron by this kind of atom is known to produce sharp spectral features which can be assigned as resonance states. The behavior of photons trapped in a defect in a finite-sized PC is similar to that of electrons in an atom mentioned above. In a manner similar to the atom, we assume that several defect states are present in the PC. The photons are confined around the defect in the PC, because the defect creates defect modes within the photonic band gap that never permit the presence of photons. Therefore, the photon has a larger field near the defect and decays exponentially toward the periphery of the finite-sized PC. The photonic field does not vanish even outside the PC, since the lower refractive index of the surrounding medium (the unity for the air) does not prohibit the presence of photons. As a result, the photonic field near the defect inside the PC is coupled to the continuous photonic field outside. This is an analogy to the electronic tunneling phenomenon mentioned above. This photonic defect state may be regarded as a photonic quasibound state and therefore its spectrum must be broadened in the vicinity of the resonance frequency. To determine the photon lifetimes for the defect states in the PC, we assume real dielectric constants (i.e., no optical gain or loss) for the rods and a complex photon frequency $\omega = \omega' - i\omega''$. According to the resonance scattering theory, the frequency dependence of the amplitude of the scattered wave follows the Breit-Wigner formula [60] and the first-order pole of the scattered-wave amplitude gives the complex frequency $\omega_m = \omega'_m - i\omega''_m$ for the resonance mode. Hereafter, we use the subscript m to indicate the specific mode obtained. Since the scattering amplitude has to diverge at $\omega = \omega_m$ irrespective of position $\mathbf{r}$ in $\boldsymbol{\varphi}(\mathbf{r})$ in Eq. (1), this divergence must occur in vector $\mathbf{b}$. This implies the condition that $\det(T) = 0$ determines the complex frequency ω_m. The photon lifetime of the relevant mode is given by $\tau_m = 1/2\omega''_m$ (and the Q factor is given by $\omega'_m\tau_m$, if necessary).

Here, we refer to the physical meaning of the above method for determining the photon lifetimes. The imaginary part ω''_m of the complex frequency thus determined must be positive since the lifetime is positive. The positive ω''_m means that k''_m is positive due to the relation $\omega_m = ck_m$ in the air, i.e., $\omega'_m - i\omega''_m = c(k'_m - ik''_m)$, where $k_m = k'_m - ik''_m$ is the complex wave number and c is the light velocity (the positive value). Since the 2D scattered wave behaves like $\exp(ik_m r)/\sqrt{r} = \exp(ik'_m r)\exp(k''_m r)/\sqrt{r}$ at large r, we find that it diverges at the limit of $r \to \infty$ because $k''_m > 0$. This may appear to be unusual, because it is as if light is amplified despite the absence of optical gain in the present physical system. Note, however, that this is true. This actually occurs because the resonance state decays exactly at this resonance frequency to magnify the light intensity outside the PC (not due to gain). In this consideration, the temporal variation of the field should be taken into account at the same time: the light field decreases with the factor $|\exp(-i\omega_m t)| = \exp(-\omega''_m t)$ since $\omega''_m > 0$. The overall behavior of the light field is described by the product of the two factors: the increasing spatial part and the decreasing temporal part. The total light field is thus known to remain unchanged at the simultaneous limits of $r \to \infty$ and $t \to \infty$. We find that the light field energy is conserved during the whole decaying process of the resonance states. This is in marked contrast to the case where the PC has optical gain and therefore the light field energy in the total system is amplified.

C. Fano resonance for the scattering cross-section

The scattered light field given by Eq. (1) has the asymptotic form $f(\theta)\exp(ikr)/\sqrt{r}$ at $r \to \infty$. We obtain the total scattering cross section σ, or the integrated far-field intensity in the terminology of quantum electronics, by integrating the scattering amplitude squared over the incident direction:

$$\sigma = \frac{4}{k}\sum_{l'=-\infty}^{\infty}\left|\sum_{l=-\infty}^{\infty}\sum_{n=1}^{N} b_{nl}e^{i(l-l')\chi_n}J_{l'-l}(kR_n)\right|^2. \tag{3}$$

All photonic modes formed in the finite-sized PCs—the quasicontinuously distributed modes in the photonic bands as well as the localized defect modes in the band gaps—can be regarded as resonance states. However, the band modes are so densely distributed that they cannot be separated from each other, which makes it difficult for us to clarify their resonance structures from their σ spectra. In contrast to this, since the defect modes are isolated in the band gaps, they will provide an ideal stage for the investigation of the photonic resonance phenomena. Hereafter, we therefore focus on the isolated defect states. The cross section of the resonance scattering by an isolated state can be described using the Fano-Beutler resonance formula in the vicinity of the isolated resonance mode ω'_m,

$$\sigma = \sigma_r\frac{(x+q)^2}{x^2+1} + \sigma_b + \sigma_c x, \tag{4}$$

where the mode frequency is normalized by the equation $x = (\omega' - \omega'_m)/\omega''_m$, and $\sigma_b + \sigma_c x$ indicates the background scattering cross section that is approximated as a linear curve near the resonance frequency. Here q is what we call the q value that was introduced by Fano [43] as an index that represents the degree of asymmetry of the resonance spectrum; this value ranges from $-\infty$ to $+\infty$, depending on the spectrum shape. Hereafter, however, we will use its inverse form q^{-1} instead of q as a matter of convenience. It is clear from Eq. (4) that the resonance spectrum is asymmetric with a peak at the lower ω' side ($x < 0$) when $q^{-1} < 0$, symmetric (mountain-shaped) when $q^{-1} = 0$, asymmetric with a peak at the higher ω' side ($x > 0$) when $q^{-1} > 0$, and symmetric (valley-shaped) when $q^{-1} = \pm\infty$. Here, for $q^{-1} = 0$ (though $\sigma_r q^2$ is finite), Eq. (4) evidently corresponds to the Breit-Wigner formula with no interference.

According to the Fano theory, the parameter q^{-1} can be regarded as an index that indicates the ratio of the probability amplitude for the transition from the initial state to the continuous-states to that to the modified-discrete-states. Here, the modified-discrete state is a discrete state modified by an admixture of the continuous states. We simply call it the resonance state in this paper. It may hence be paraphrased that the parameter q^{-1} is the ratio of the probability amplitude for the excitation to the continuous-states to that to the resonance-states. By this definition, the relation $q^{-1} = 0$ implies that the resonance scattering is the primary contribution to the scattering cross section, while the relation $q^{-1} = \pm\infty$ implies that the direct scattering to the continuous states is dominant in the σ spectrum. The moderate q^{-1} values that are of the order of ± 1 suggest a presence of the pronounced interference between these two kinds of scattered waves. These q values will be used in Sec. III B to characterize the resonance structures of intrinsic defect states created in the PCs.

III. RESULTS

In this paper, we used GaAs as the material of rods with the dielectric constant $\varepsilon_a = 13.18$ and the air as the background material ($\varepsilon_b = 1.00$). The PCs studied are finite-sized crystals with a hexagonal lattice and symmetric external form, as shown in the inset of Fig. 1(a). The structural parameters are fixed at $N = 61$ for the number of rods and $f = 0.3$ for their filling factor. We used typically 27 partial waves ($-13 \leqslant l \leqslant +13$) for the l expansion in Eq. (1), which warranted the sufficient convergence of the series. In this paper the numerical values of all physical quantities are represented in the dimensionless normalized form: the angular frequency ω is normalized in units of $2\pi c/L$, the photon lifetime τ in units of L/c, and the atomic displacement d and the scattering cross section σ in units of L, where L is the lattice constant of the PC.

A. Formation of intrinsic defects

Prior to entering into the description of the defects, we show in Fig. 1(a) the photonic band diagram of the present PC with

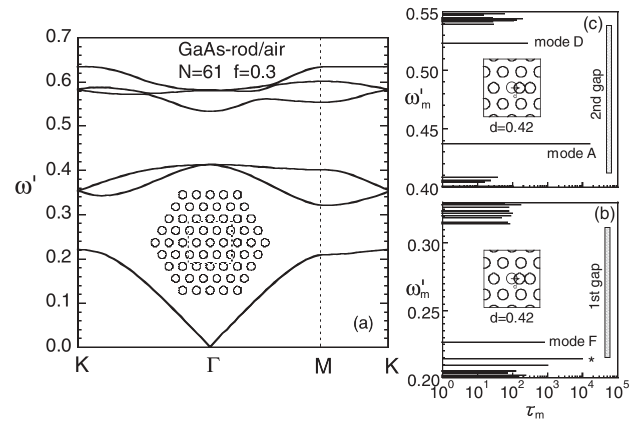

FIG. 1. (a) Photonic band diagram computed for the PC with an infinite number of unit cells (the rod filling factor is $f = 0.3$). Here, ω' is the real part of the complex angular frequency $\omega = \omega' - i\omega''$, which is normalized in units of $2\pi c/L$ (L is the lattice constant). The inset shows the finite-sized PC consisting of 61 rods without imperfections. (b) Frequency positions ω'_m and lifetimes τ_m for the modes around the first gap of the PC with a defect created by displacing the central rod by $d = 0.42$ (see the inset). (c) Similar results for the modes around the second gap.

no defects, which was calculated by the plane-wave expansion method assuming the infinite number of rods. Here, ω' is the real part of the complex angular frequency $\omega = \omega' - i\omega''$. In this paper, we focus on the frequency regions in which two band gaps are observed. We created an intrinsic defect by displacing a rod atom from the regular site (the central lattice point in the PC) toward the neighboring rod. This defect is hence composed of a vacancy and an interstitial rod. The insets in Figs. 1(b) and 1(c) portray the defect of this type where the central rod is displaced by d from the original position (the dotted circle). See also the region surrounded by the dotted line in the inset in Fig. 1(a), which corresponds to the insets in Figs. 1(b) and 1(c). For the defect in these figures, we used $d = 0.42$, the possible largest value that can avoid intersecting with the neighboring rod. This defect was found to generate three distinct defect modes, i.e., one in the first gap and two in the second gap. Figure 1(b) shows the frequency positions ω'_m and the lifetimes τ_m for the modes created around the first gap. We find an isolated defect mode ($\omega'_m = 0.226\,136$) above the top of the first band; let us call it mode F. In addition, a high-τ_m mode is detected near the bottom of the band edge, as shown by an asterisk, which we will refer to later. We can see a lot of modes densely distributed outside the gap, which are the Bloch states—discretized due to the finite size of the PC—in the first and second photonic bands. Figure 1(c) shows the results around another gap. As clearly shown in Fig. 1(c), two defect modes are found to be created within the band gap: one mode is located above the top of the lower band ($\omega'_m = 0.436\,781$) while another mode is below the bottom of the upper band ($\omega'_m = 0.522\,826$). Because of their frequency positions, we could call them the acceptor (mode A) and donor (mode D) states, as they are occasionally called in the body of PC research by analogy with the impurity states in semiconductors [29,61]. Three different defect states are thus known to be simultaneously created in a single defect structure.

The above results are summarized in Fig. 2, which shows the variations of the mode frequency ω'_m(closed circles) and the lifetime τ_m (open circles) for (a) mode F, (b) mode A, and (c) mode D as a function of the atomic displacement d. Figure 2(a) includes the results for the mode shown by the asterisk in Fig. 1(b) as well, which are displayed using small closed squares (ω'_m) and small open squares (τ_m). The $d = 0$ results are obviously meaningless if they are considered as the defect mode data, since the PC with no displaced atoms is perfect: these data were merely taken from the modes formed at the extreme ends of the photonic bands. Let us first look at the results in Figs. 2(b) and 2(c) as a matter of convenience. As clearly seen in these figures, the states created for $d \neq 0$ appear to converge at the states at $d = 0$. It is speculated from this fact that these band-edge states seen for $d = 0$ work as the seeds for generating the defect states. As shown in Fig. 2(b), mode A is leaving the top of the third photonic band by the atomic displacement and is deeply driven into the band gap to make a more localized authentic defect mode (deep acceptor state). The same phenomenon occurs for mode D, which is leaving the fourth photonic

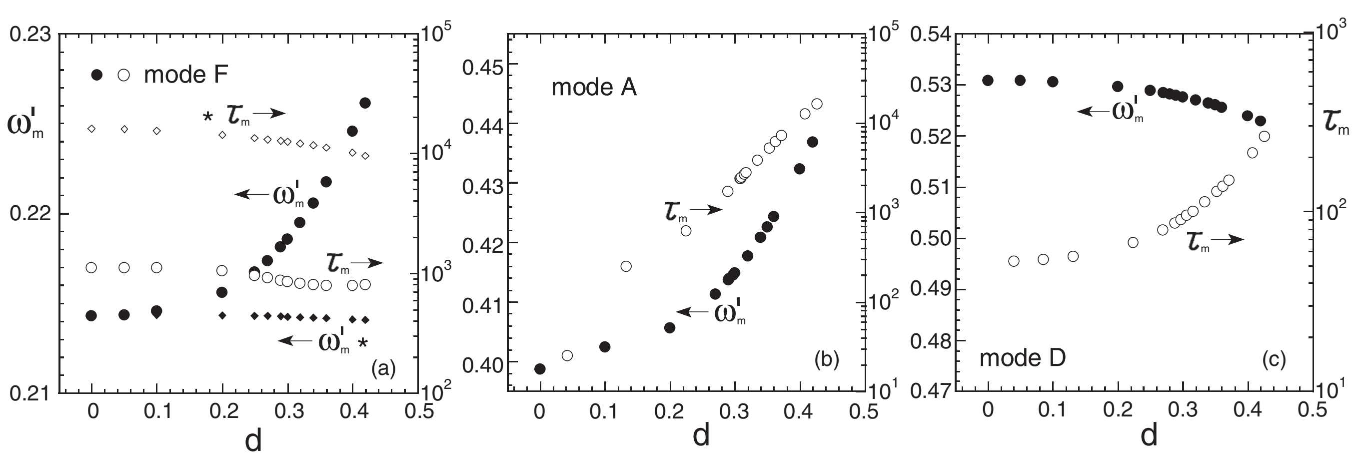

FIG. 2. Mode frequency ω'_m and photon lifetime τ_m for the modes created as a function of the rod displacement d for (a) mode F and mode * in the first gap, (b) mode A in the second gap, and (c) mode D in the second gap. Here, τ_m and d are measured in units of L/c and L, respectively.

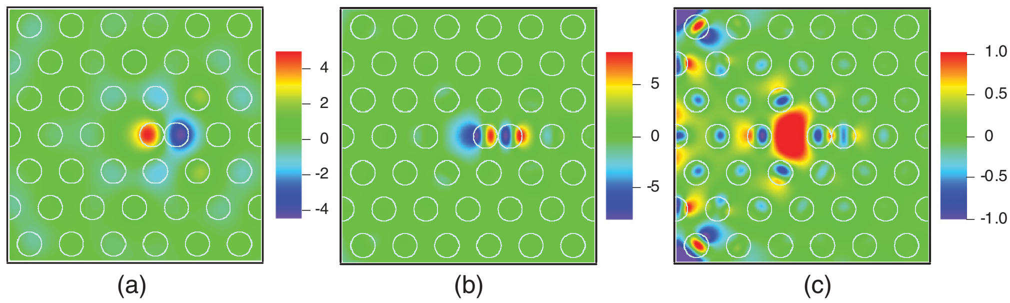

FIG. 3. (Color online) Electric field distributions in the vicinity of the defect ($d = 0.42$) at each mode frequency ω'_m for (a) mode F, (b) mode A, and (c) mode D. Here, the PC is irradiated with the plane wave of light sent from the left.

band though its frequency variation is much smaller than that of mode A for the same displacement. Mode A exhibits a rapid increase in the photon lifetime [as shown in Fig. 2(b)] with the increasing atomic displacement, and it reaches the highest value $\tau_m = 1.63 \times 10^4$ for the maximally deformed configuration ($d = 0.42$). In contrast to this, mode D shows only a slight enhancement in the lifetime: we thus find that this donor state is less sensitive to the disorder than the acceptor state. The variations of ω'_m and τ_m displayed in Figs. 2(b) and 2(c) suggest the presence of a systematic correlation between them. Here, we define $\Delta\omega'_m$ and $\Delta\tau_m$ by the deviations of the values from those at $d = 0$: $\Delta\omega'_m \equiv |\omega'_m(d) - \omega'_m(0)|$ and $\Delta\tau_m \equiv \tau_m(d) - \tau_m(0)$, respectively. By the numerical fitting, we find that the correlations between them are well expressed by the empirical equations: $\log_{10}\Delta\tau_m = 6.81 + 1.87\ \log_{10}\Delta\omega'_m$ for mode A, while $\log_{10}\Delta\tau_m = 5.23 + 1.42\ \log_{10}\Delta\omega'_m$ for mode D. From the fact that the prelog factor for mode A (1.87) is larger than that for mode D (1.42), we understand that $\Delta\tau_m$ is a more sensitive function of $\Delta\omega'_m$ for acceptor states. We thus know that these defect states are simultaneously created and their mode frequencies and lifetimes are widely tuned merely by displacing a single rod from the regular position. We next move back to Fig. 2(a), which depicts the variations of ω'_m and τ_m for the two modes near the top of the first band. In contrast to the modes in the second gap, these modes show somewhat unusual behavior, as follows. First, mode F is driven into the photonic gap, leaving the edge of the first band with the increasing atomic displacement, which is reasonable when we regard it as a defect mode. However, it has a lifetime (1.2×10^3) at $d = 0$ which is very high as the lifetime for the band-edge mode. Compare it to those for the band-edge modes in Figs. 2(b) and 2(c) (2.0×10^1 for mode A and 5.0×10^1 for mode D). Moreover, we find that its lifetime remains nearly constant with the change of the atomic displacement, whereas its mode frequency deeply penetrates into the band gap. Second, the mode denoted by an asterisk in Fig. 2(a) does not change its mode frequency as well as its lifetime by the atomic displacement. This clearly indicates that it is a band mode, which has been confirmed by the study of the light-field distributions: light is extended over the whole PC for all atomic displacements. However, its lifetime (about 1.5×10^4) is very high; in particular, note that it is much higher than that for the localized defect mode F (about 1.2×10^3). From these facts, we should not hold back from concluding that this mode—evidently a band-edge mode—is superior to the localized defect mode for confining light.

In order to investigate these defect states in more detail, we calculated the electromagnetic fields around the defect. Figure 3 displays the distributions of the electric field of light [the real part of $E^s(\mathbf{r})$] for (a) mode F, (b) mode A, and (c) mode D, which have been created by the maximal atomic displacement ($d = 0.42$). Here, the incident angle is chosen as 0°. As shown in the color scale, the field is depicted using the different scales for each figure. In all figures we see the concentration of light toward the intrinsic defects. When we look into them more precisely, we find that the light localization occurs around the displaced rod for modes F and A, while it occurs within the vacancy created by the rod displacement for mode D. Moreover, we find that modes F and A have stronger localized-field intensities than mode D by a factor of 25 ($= 5^2$) to 64 ($=8^2$), as known from the color scale. Light is thus known to be more strongly confined in acceptor states (modes F and A) than the donor state (mode D).

B. Fano resonance profiles for scattering cross sections

Before displaying the detailed resonance properties of defect states, here we discuss all the PC modes (the band modes as well as the defect modes). Figure 4 shows the spectrum of the

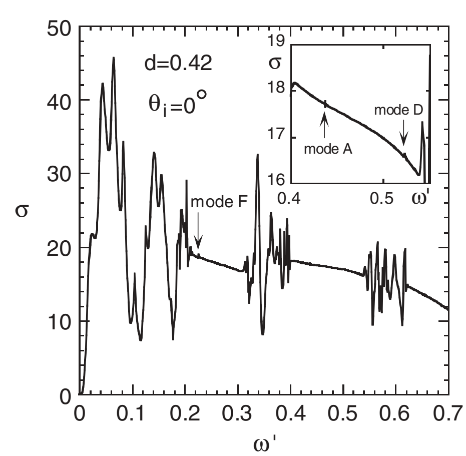

FIG. 4. Spectrum of the total scattering cross-section of light scattered by the present finite-sized PC with an intrinsic defect formed by the displacement $d = 0.42$. Here, the incident angle is $\theta_i = 0^\circ$. The inset shows the spectrum magnified around the second photonic band gap. The peak in this figure corresponds to mode F, and the tiny peaks seen in the inset are assigned as modes A and D. The scattering cross-section σ is normalized by L.

total scattering cross-section for light scattered by the finite-sized PC with a defect created by the atomic displacement $d = 0.42$. Here, the incident light is sent from the left side of the PC ($\theta_i = 0°$). The light frequency ω' and the scattering cross section σ are normalized to $2\pi c/L$ and L, respectively. In the long-wavelength limit ($\omega' \to 0$), the scattering is weak because the target becomes much smaller than the wavelength in this ω' region. When ω' increases from 0, then σ rapidly increases and exhibits a complicated spectrum. We see three plateaus in the σ spectrum. These monotonic σ variations indicate the occurrence of the scattering by a rigid body that has no internal states. Moreover, we find that these plateaus coincide very well with the photonic band gaps computed for the infinite-sized PC (see Fig. 1). The frequency regions showing σ plateaus can therefore be regarded as the photonic band gaps. The numerous peaks seen in the spectrum evidently come from the band modes that have been discretized due to the finite size of the PC. As discussed before (Sec. III A), these modes are also some kind of photonic resonance modes, but they have relatively short lifetimes because they are the extended states (the Bloch states) that are coupled less weakly to the continuous states outside. The minute examination of the spectrum has isolated one resonance state within the first gap and two resonance states within the second gap. The latter two states are more clearly displayed in the inset (the magnified spectrum near this region). These three resonance states can be identified as mode F, mode A, and mode D, respectively, presented in Fig. 1, because their frequency values exactly coincide with those shown in Fig. 1. From the results displayed here, we feel certain that the scattering cross-section spectrum is a useful tool to visualize the presence of photonic modes (particularly, defect modes) and estimate their locations on the frequency axis. This is because the scattering cross-section spectrum requires no time-consuming calculations compared with those for determining the resonance modes accurately (as described in Sec. II B). Moreover, as will be clarified in the

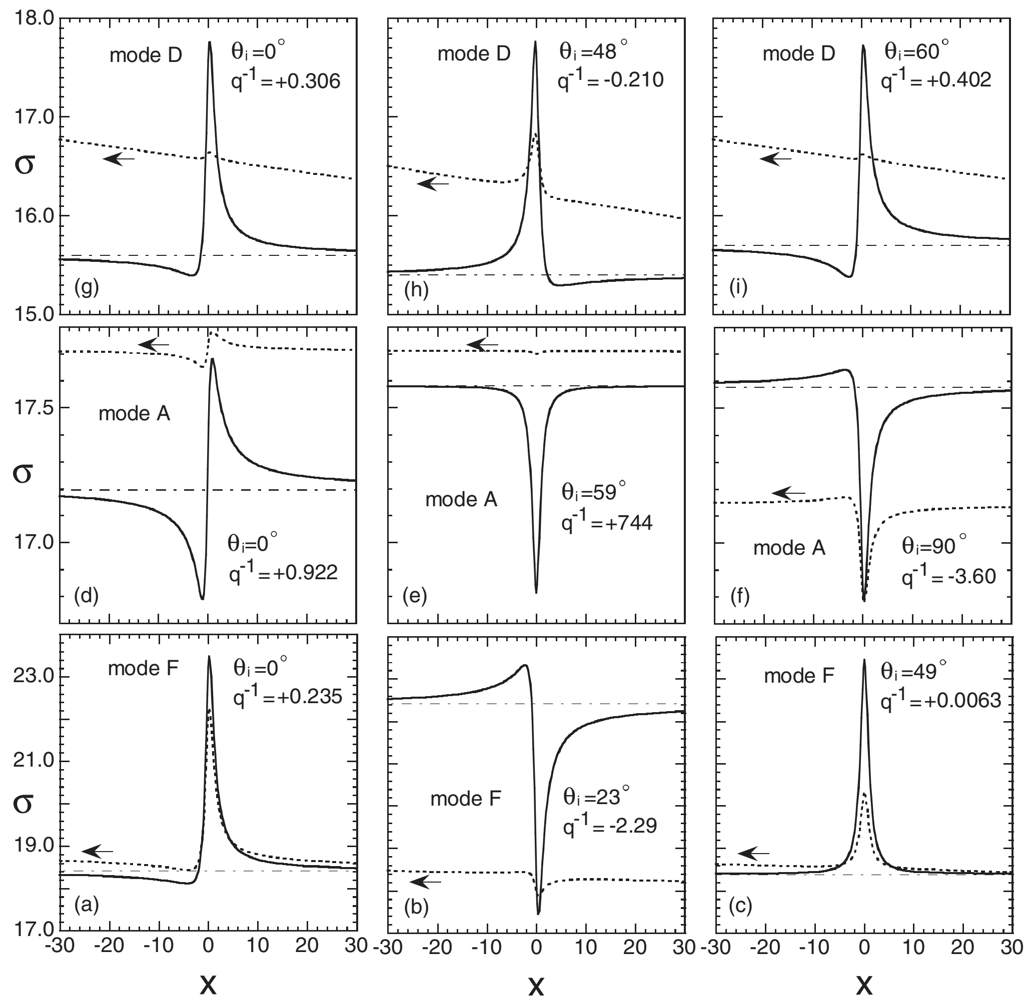

FIG. 5. Total scattering cross-section spectra in the vicinity of the mode frequency for the intrinsic defect formed by the atomic displacement $d = 0.42$ for (a)–(c) mode F, (d)–(f) mode A, and (g)–(i) mode D. Here displayed are those for typical incident angles which show a variety of scattering cross-section spectra. The dotted lines are the as-computed raw data of the scattering cross-section (see the left scale). The solid lines indicate the spectra normalized by subtracting the background from the raw data, where we used the arbitrary scale for these lines. These figures also display the q^{-1} values obtained by fitting the scattering cross-section spectrum to the asymmetric resonance line profile given by Eq. (4).

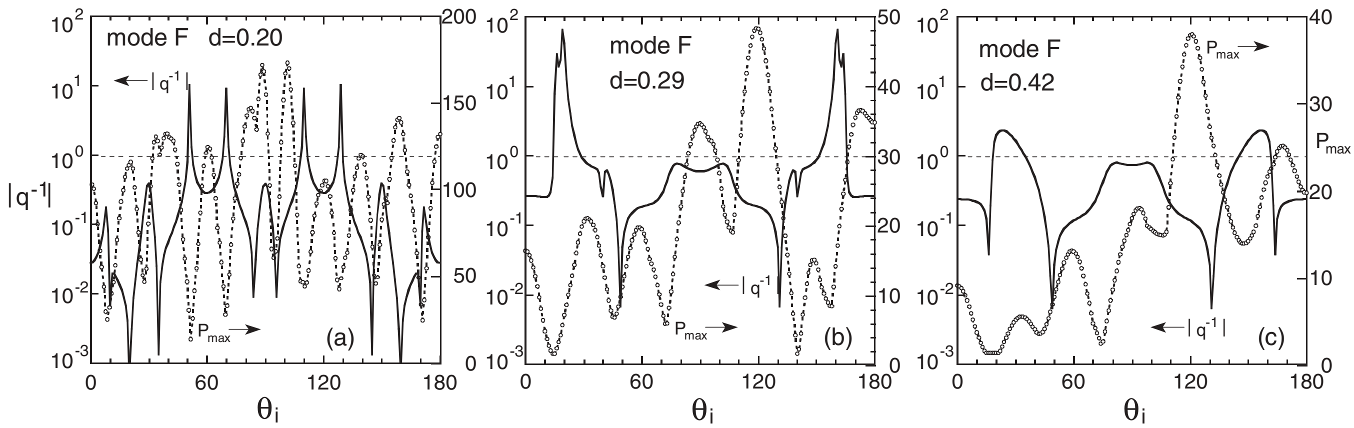

FIG. 6. $|q^{-1}|$ value (solid line) and $P_{\max}$value (open circles and dash-dot line) as a function of the incident angle θ_i determined for mode F created by the rod displacements of (a) $d = 0.20$, (b) $d = 0.29$, and (c) $d = 0.42$. Here, q is the so-called Fano value that indicates the asymmetry of the resonance spectrum and $P_{\max}$ is the maximum value of the time-averaged Poynting vector within the PC.

succeeding paragraphs, it provides us information concerning the resonance properties of defect states through the analysis of the scattering cross-section line profiles.

We display in Fig. 5 several examples of the total scattering cross section σ as a function of the normalized frequency x, which are magnified in the vicinity of the defect mode: (a)–(c) for mode F, (d)–(f) for mode A, and (g)–(i) for mode D under the irradiation of light from several different directions. All of these figures are for the defect with the atomic displacement $d = 0.42$, and the incident directions of light are so chosen that they provide a variety of σ profiles. Here, x is the frequency converted by the equation $x = (\omega' - \omega'_m)/\omega''_m$, where ω'_m and ω''_m are real and imaginary parts, respectively, of the complex frequency for the relevant defect mode computed. See Sec. III A for ω'_m values. The broadening factors are computed to be $\omega''_m = 0.0\,000\,992\,696$ for mode F, $\omega''_m = 0.00\,000\,489\,646$ for mode A, and $\omega''_m = 0.000\,305\,834$ for mode D. While the broadening factor thus depends strongly on the mode under consideration, all the spectra in Fig. 5 are so displayed that they have the same broadening as a result of the conversion of the abscissa mentioned above. The dotted lines are the scattering cross-section spectra that have the values measured by the scale in the ordinate. The solid lines indicate the spectra obtained by subtracting the background from the scattering cross-section spectra (dotted lines), and they are displayed in the arbitrary units. The dash-dot lines are the zero levels of the spectra shown by solid lines. These spectra have thus been found to have distinct asymmetric Lorentz resonance profiles, although they emerged at first as the tiny modulations of the gap-related plateaus (Fig. 4). As displayed in Fig. 5, these defect states exhibit line profiles, the forms of which are very different depending on the incident direction. These forms may be grouped into four classes: (1) symmetric normal resonance, (2) symmetric antiresonance, (3) asymmetric resonance with a peak at higher x, and (4) asymmetric resonance with a peak at lower x. For modes F and A, we notice that the resonance profiles exhibit a drastic change according to the incident light direction. On the other hand, mode D hardly shows any change in its profile for the wide variation of the incident direction. These profiles have been successfully fitted to Eq. (4) by using appropriate q values with very small relative σ errors of the order of 10^{-4} at every x point; the q^{-1} value is indicated in each figure.

Let us next make a systematic study of the q values for a variety of σ profiles. Figure 6 shows the absolute q^{-1} value ($|q^{-1}|$, shown by solid lines) as a function of the incident angle θ_i for mode F created by displacing the rod by (a) $d = 0.20$, (b) $d = 0.29$, and (c) $d = 0.42$. We do not mention here the results shown by open circles and the dash-dot line in this figure and keep them for the later discussions (Sec. IV B). In Fig. 6, the q^{-1} sign changes at every angle at which $|q^{-1}|$ vanishes or diverges. Since all the σ spectra for mode F have positive q^{-1} values at $\theta_i = 0^\circ$ (e.g., $q^{-1} = +0.235$ for $d = 0.42$), we can know their signs at every incident angle starting from $\theta_i = 0^\circ$. However, we ought to note here that it hardly gives us any important information whether the sign of the q value is positive or negative: at least, we should say that its physical meaning is not understood at the current stage of the research of the Fano resonance. Hence, we consider only the absolute values of q^{-1}. As shown in Fig. 6, the $|q^{-1}|$ value exhibits a somewhat complicated and rapid variation with the change in the incident direction of light. While it falls suddenly to tiny values at several specific angles, it rises sharply to nearly infinite values at other angles. The extreme sensitivity of q^{-1} to the incident angle suggests the presence of the incident-direction-dependent, optical-resonance processes. Although any decisive differences can barely be found in the $|q^{-1}|$ variation between Figs. 6(b) and 6(c), we notice that it comes to have fine structures for the decreased rod displacement. These $|q^{-1}|$ variations in Fig. 6 appear to be symmetric around the angle of 90°. The detailed study, however, shows that it is slightly asymmetric (with a relative error of 10^{-2}) between 0° and 180°. This is evidently caused by the asymmetry—though it is a small contribution to the whole PC—of the defect structure with respect to the mirror reflection at the vertical line passing the center of the PC. Actually, the degree of the asymmetry in the $|q^{-1}|$ variation is found to be reduced as the defect becomes more symmetric by decreasing the rod displacement.

The $|q^{-1}|$-θ_i relations for mode A are displayed in Fig. 7 for (a) $d = 0.20$, (b) $d = 0.29$, and (c) $d = 0.42$. Here,

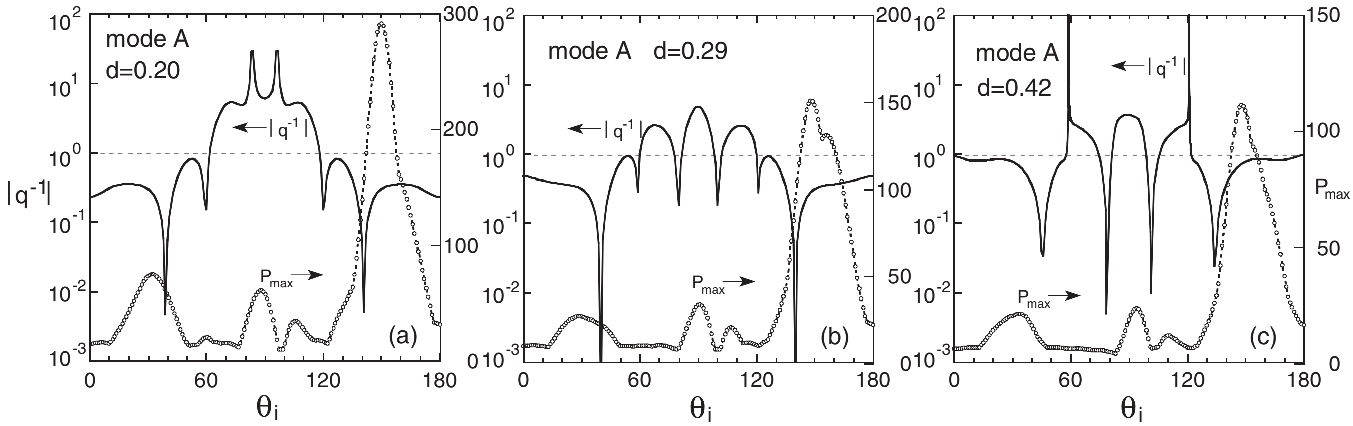

FIG. 7. $|q^{-1}|$ value (solid line) and $P_{\max}$ value (open circles and dash-dot line) as a function of the incident angle θ_i determined for mode A created by the rod displacements of (a) $d = 0.20$, (b) $d = 0.29$, and (c) $d = 0.42$.

again, we discuss the other data (open circles and dash-dot line) later (Sec. IV B). As we can see in Fig. 7, we hardly find any differences in the $|q^{-1}|$ variations at lower angles ($0^\circ < \theta_i < 60^\circ$) as well as higher angles ($120^\circ < \theta_i < 180^\circ$) between different atomic displacements. In the intermediate region ($60^\circ < \theta_i < 120^\circ$), however, we find that this variation exhibits remarkable transformations. Despite its complicated behavior, however, we can clearly recognize a reasonable $|q^{-1}|$ metamorphosis associated with the atomic displacement. It would enable us to understand its variation more easily to start the consideration from the structure with the intermediate displacement, i.e., $d = 0.29$. First, let us look at the $|q^{-1}|$ transformation by increasing d from 0.29 to 0.42. By increasing d, the angles 60° and 120°—geometrically critical angles—emerge as the singular points in Fig. 7(c), which make the $|q^{-1}|$ value diverge to infinity. This singularity has been hidden as a result of being softened due to the small displacements for the defects with $d = 0.20$ and 0.29. In the intermediate region ($70^\circ < \theta_i < 110^\circ$), we find no significant difference in the $|q^{-1}|$ variation between Figs. 7(b) and 7(c), except for the difference in the q^{-1} sign. Next, we examine the transformation by decreasing d from 0.29 to 0.20. The notable phenomenon that occurs by decreasing d is the appearance of the singularity near the angles of 83° and 97°. Other features appear to remain unchanged: the small peak near 70° for $d = 0.29$ still exists for $d = 0.20$ and the negative q^{-1} value at 90° is still negative for $d = 0.20$. This complicated behavior, compared with the relatively simple one for mode D (as will be mentioned later), is supposed to arise from the complicated wave function of mode A, which is characterized by several nodes and loops and the wave form elongated along the horizontal axis [see Fig. 3(b)]. Due to this asymmetric wave function, mode A can be regarded as possessing nonvanishing angular momentum. This property of mode A will undoubtedly make its coupling to the directly scattered waves intricate and hence the angle dependence of σ complicated. In other words, this acceptor state appears to work as an active center, which would cause a pronounced interference with the directly scattered waves. The angle-resolved q value for this state is thus known to be very sensitive to the atomic displacement. From the above results, we believe that the measurement of the q values would be a useful tool for elucidating the relation between the defect structure and the resonance properties.

Similar studies have been conducted for the $|q^{-1}|$-θ_i relations for mode D, as shown in Fig. 8. As seen in Fig. 8, the $|q^{-1}|$ value oscillates with the incident angle, indicating

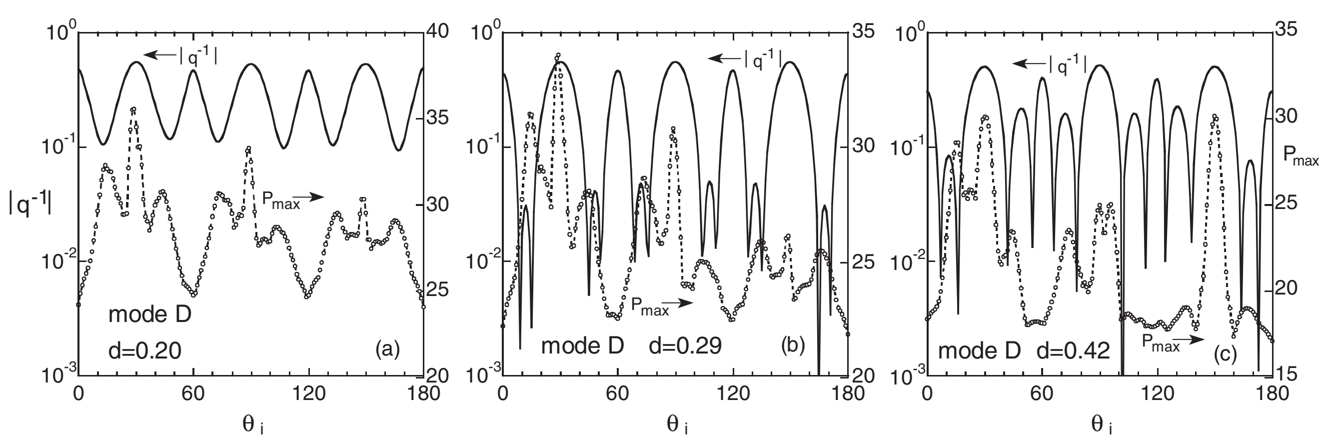

FIG. 8. $|q^{-1}|$ value (solid line) and $P_{\max}$ value (open circles and dash-dot line) as a function of the incident angle θ_i determined for mode D created by the rod displacements of (a) $d = 0.20$, (b) $d = 0.29$, and (c) $d = 0.42$.

the periodic variation of the interference between mode D and the background waves. We note, however, that its variation is similar to each other between the samples with different atomic displacements, which could be displayed more distinctly by using the linear scale for $|q^{-1}|$. The only difference is that, as the rod atom is displaced further, i.e., the defect disorder is increased, the q^{-1} value shifts to the negative side and its oscillation amplitude is magnified. All the q^{-1} values in Fig. 8 remain in a small-$|q^{-1}|$ range ($-0.2 < q^{-1} < +0.5$). This appears to come from the fact that this state has a less deformed field distribution—an approximately spherically symmetric state with null angular momentum—around the defect [see Fig. 3(c)].

IV. DISCUSSION

A. Characteristics of intrinsic defects

The photon lifetimes of modes A and D shown in Figs. 2(b) and 2(c) are well correlated with the mode frequency positions in the band gap. Actually, the photon lifetime is magnified due to the attenuated coupling of the defect states with the outer continuous states, which occurs as the defect states get separated further from the Bloch states (the extended states in the bands) and driven toward the midgap more deeply. The photon lifetime for mode A reaches the maximum value that is a 10^3 order of magnitude longer than those for the band-edge modes ($d = 0$). However, this value is shorter than those obtained in more sophisticated structures of similar sizes, such as circulating Bloch modes in a photonic atoll [11,12] and WGMs in a single microstructure [13–17]. From the results in Figs. 2(b) and 2(c), we expect that the d increase toward $d > 0.42$ will bring a further enhancement in the photon lifetime. At the current stage, the method described in Sec. II unfortunately is unable to calculate the d region where the displaced rod merges into the neighboring rod. However, the extreme case ($d = 1$) can be calculated, for which the displaced and neighboring rods overlap each other completely and as a result, a rod vacancy is created at the central site of the PC with the reduced number of rods ($N = 60$). In this case, we observe the creation of a single mode with $\omega'_m = 0.475\,615$ and $\tau_m = 9.49 \times 10^3$. This τ_m value is of the order of half the highest value obtained for the defect mode formed by the atomic displacement. These results are consistent with the field distributions shown in Figs. 3(b) and 3(c). The interesting point here is the region around which light is concentrated. We recognize that mode D is localized in the vacancy (the air) produced by the atomic displacement, while mode A is localized mostly within the rods (the dielectric material). These results are reasonably understood as follows. Mode A (acceptor)—occupying a lower energy level in the photonic band gap—comes to possess this lower photonic energy as a consequence of the confinement of light in the materials with higher dielectric constant, because the higher dielectric constant permits light to stay there in an energetically more stable manner. In contrast to this, the opposite is true for mode D (donor) that occupies a higher energy level, because light is confined in the vacancy (air) which gives an energetically unstable environment to light. Note for reference that the mode, the only mode,in the vacancy defect formed by eliminating the central rod atom ($N = 60$), as mentioned before, has a light distribution concentrated on the vacancy itself. It is speculated from this fact that the simultaneous formation of donor and acceptor states may be caused by a relatively complicated defect like this, which causes the localization of light either in the displaced rod or in the vacancy.

We next move on to the discussion of the unusual behavior of the modes shown in Fig. 2(a). Speaking of the very high τ_m values for the band-edge mode (asterisk), we suppose that it is closely related to the outer form of the PC. In fact, we have found the same indication as the above in the previous paper [6]; the symmetric PC with $N = 37$ had a τ_m value (6.5×10^2) higher than that (4.3×10^2) for the asymmetric PC with $N = 53$ at the band edge. There is a general rule which mentions that band-edge modes have higher lifetimes for the PCs with more rods, because more rods enhance the multiple scattering of light and hence allow light to stay in the PC for a longer time. The discrepancy between this rule and the results mentioned above is evidently caused by the difference in their outer PC forms. We speculate about it as follows. The symmetric PC gives rise to the Fabry-Pérot (FP)-type confinement because of the parallel sides in such a PC. This additional confinement effect is thought to strengthen the light confinement, which occurs in the present symmetric PC with $N = 61$ as well as the symmetric PC with $N = 37$ in the previous paper. In contrast to this, the asymmetric PC does not produce the FP confinement because of the unparallel sides in such a PC, which does not intensify the light confinement, as shown for the asymmetric PC with $N = 53$ in the previous paper. Another unusual variation (i.e., for mode F) can be explained as follows, by taking into account the intrinsic nature for the band-edge modes in the present symmetric PC as mentioned above. The band-edge modes including mode F at $d = 0$ already have the FP-assisted long lifetimes. The increasing atomic displacement drives one of the band-edge modes—for which mode F is chosen accidentally—into the photonic gap to form a localized defect mode. This is confirmed by the light-field distributions: light for this mode comes to be more localized for larger atomic displacements [see Fig. 3(a)]. However, this localization does not increase the lifetime because it is already sufficiently long, even at $d = 0$. For small atomic displacements ($0 < d < 0.3$), the lifetime for mode F displays the same variation as that for the true band-edge mode [small open squares in Fig. 2(a)]. Noteworthy, here, is that for $d > 0.3$, the lifetime for mode F is slightly augmented while the true band edge mode is not. This slight increase of τ_m is evidently caused by the lifetime as a localized defect, which has come to the surface because of the large atomic displacements. This kind of phenomenon does not occur for the modes in the second gap, possibly because the higher-order Bragg reflections would complicate the processes of the lifetime enhancement.

B. Resonance structures of intrinsic defects

First, we mention the results shown by open circles and the dash-dot line in Figs. 6–8, which we did not refer to in Sec. III B. On the basis of the studies conducted before [58], we presumed that the resonance structures characterized by the q

values may be closely linked with the influx of light energy into the localized states. The minute examination has been carried out for the distributions of the optical energy flow in the PCs at the defect mode frequency. The open circles and dash-dot line in these figures indicate the $P_{\max}$ values—the maximum values of the time-averaged Poynting vector within the PC—under the irradiation with the incident angle θ_i. In what follows, we discuss the correlations among the q values, the $P_{\max}$ values, and the resonance processes for each defect state.

In Fig. 6 for mode F, we find a pronounced dependence of the $P_{\max}$ value upon the incident direction. First, we note that the cycle of the $P_{\max}$ variation is similar to that of the $|q^{-1}|$ variation, which suggests the presence of a correlation between the resonance property of the defect and the energy flux of light. Noteworthy here is that not all but many of the $P_{\max}$ peak positions approximately fall on the incident angles at which the $|q^{-1}|$ value vanishes. For example, the maximum $P_{\max}$ occurs at $\theta_i = 20^\circ$ for (a), $\theta_i = 57^\circ$ for (b), and $\theta_i = 166^\circ$ for (c), which nearly coincide with the angles that cause $|q^{-1}| \approx 0$, i.e., $\theta_i = 21^\circ$ for (a), $\theta_i = 50^\circ$ for (b), and $\theta_i = 164^\circ$ for (c), respectively. Other extrema points also coincide with each other with an error of about 10°, which should be regarded as good agreement when these angles are considered in the whole wide range $0^\circ - 180^\circ$. Let us hereafter call them the $|q^{-1}|$-extrema angles. From the investigation of the Poynting vector distributions in the PC, we have learned that the most rapid streams, i.e., those giving the greatest $P_{\max}$, are created by light coming into the defect. In other words, under the irradiation from these $|q^{-1}|$-extrema directions, the localized defect state strongly couples to the outer states in the incoming process and as a result, permits itself to be excited more efficiently to capture more photons. The strengthened coupling may mostly be caused by the matched symmetry of the wave functions between the defect state and the outer continuous states incident from these directions. Since the $P_{\max} - \theta_i$ relation is determined by the coupling between these two states, the defect structure and its resulting wave function would have an important role. It is hence natural that the $P_{\max} - \theta_i$ relation is asymmetric across the line $\theta_i = 90^\circ$ because of the same asymmetry of the defect structure. The defect state is thus densely populated with photons because of the noticeable flows under the irradiation from these directions. The subsequent process, i.e., the relaxation of photons from the defect, therefore occurs remarkably. For this reason, the scattering process for the photons via the defect state (indirect scattering) comes to have a more significant role than the potential scattering process (direct scattering). This would make the indirect process, i.e., the resonance process, more prominent and subsequently the interference between them weak. The correlations between the $P_{\max}$ maximization and the vanishing $|q^{-1}|$ values can thus be reasonably understood.

Let us next move on to the results for mode A shown in Fig. 7. We find for this mode A as well that several $P_{\max}$-peak positions approximately fall on the incident angles at which the $|q^{-1}|$ value vanishes. However, since we find only a few angles of this kind for mode A, we should veer the discussion from a point to a region, as follows. We observe the broad spectra with high $P_{\max}$ values for the angle regions $0^\circ < \theta_i < 60^\circ$ and $120^\circ < \theta_i < 180^\circ$. These angle regions coincide well with those which give small $|q^{-1}|$ (i.e., $|q^{-1}| \ll 1$) for every atomic displacement. In addition to the above, the specific angles at which $|q^{-1}|$ vanish in these regions are found to fall on those close to the angles, with an error of about 10°, at which the $P_{\max}$ value reaches a maximum. Moreover, we find that the $P_{\max}$ value in these regions comes to be increased by reducing the atomic displacement; this correlates very well with the decreasing $|q^{-1}|$ value in the same angle regions. These correlations again confirm the conclusion drawn for mode F that the optical energy flux comes to be maximized in the environments where $|q^{-1}|$ vanishes, i.e., the resonance process exceeds the direct process.

As for mode D in Fig. 8, we focus on the discussion for the wide-angle region. We mentioned in Sec. III B that the q^{-1} value in Fig. 8 remains in a small-$|q^{-1}|$ range (i.e., $|q^{-1}| \ll 1$) throughout the incident angle for all atomic displacements. This fact indicates that there occurs no pronounced interference between direct and resonant waves and therefore the pure resonance processes are dominant ($|q^{-1}| \approx 0$). In other words, this defect mode tends to capture most all of the photons coming from any direction of the incident light beam. This fact corresponds very well to the $P_{\max}$ results shown by open circles in Fig. 8: $P_{\max}$ retains certain large values (note that the $P_{\max}$ axis does not begin at zero). It never falls to values smaller than 17 for all incident angles, and we here should stress in particular that it does not vanish at any angles. The above results clearly indicate the presence of the pronounced optical energy flux around the localized defect mode, which corresponds to $|q^{-1}| \ll 1$.

From the discussions concerning modes F, A, and D, we have derived a conclusion that the optical energy flux comes to be maximized in the environments where $|q^{-1}|$ vanishes, i.e., the resonance process exceeds the direct process. This conclusion holds for all of three defect states. However, we feel that it applies to mode F more precisely than modes A and D. This is, we speculate, because mode F is created in the first gap while modes A and D are created in the second gap. The band gaps with higher indices are generated by the higher-order Bragg-reflection, the interference in which ought to be more complicated than that in the lowest gap. This undoubtedly would make it more difficult to understand modes A and D than mode F.

To conclude the discussion, we would like to mention the following two points. The first point is concerning $|q^{-1}| = \infty$. The correlations between the $P_{\max}$ maximization and the vanishing $|q^{-1}|$ values have been reasonably understood in the preceding paragraphs. However, little is understood at the current stage of investigation as to the angles at which the $|q^{-1}|$ value diverges (antiresonance), which we have disregarded in this paper as a result of focusing on $q^{-1} = 0$. Some elaborate considerations will be needed, for example, based on the analogy with the similar phenomena, e.g., in the electric LCR parallel circuits (which consist of inductance L, capacitance C, and resistance R), in order to physically understand the antiresonance phenomena in the optical Fano effects. The second is about the structure of the defect. In this paper we have studied a single defect that is of a relatively simple structure. The Fano resonance for more complicated defects will become another interesting research field. In particular, the coupled two identical defects embedded in the PCs will form an optical molecule that has the states similar to the electronic bonding and antibonding states. The study of Fano effects for this artificial molecule may provide the BIC (the bound state in the continuum) [62] for the antibonding state, i.e., the state with the infinite lifetime. This state is sufficiently isolated from the environment and therefore it will make a high-quality optical resonator with very long lifetime.

V. SUMMARY AND CONCLUSION

Theoretical investigations have been carried out for the intrinsic point defects created by displacing a single rod atom from its regular site in the two-dimensional finite-sized photonic crystals with the hexagonal lattice. This paper focuses on the formation processes and the resonance properties of the defects thus created. First, the mere displacement of a single rod atom was found to create simultaneously a defect mode within the first gap and two defect modes within the second gap. The two defect states in the second gap were called acceptor and donor states by analogy with the impurity states in semiconductors, because they emerged in the photonic gap above the top of the lower band and below the bottom of the upper band, respectively. The lifetimes of light trapped at these defect states can be tuned in a wide range (on the order of 10^3) by adjusting the position of the displaced rod appropriately. These light-confinement phenomena have been reasonably explained in terms of the stability of light. On the other hand, the defect in the first gap showed an anomalous behavior: it exhibited a long lifetime even for its seed state at the band edge, i.e., the state with no atomic displacement, and its lifetime remained nearly constant by increasing the atomic displacement. This behavior was plausibly explained by taking into consideration the Fabry-Pérot confinement due to the symmetric external form of the present photonic crystals. The present method for tuning lifetimes has an advantage over the other methods, e.g., inserting an extrinsic rod atom, because the former requires only the lithographical technique for the same dielectric materials while the latter needs to handle other materials in addition. We therefore believe that the reconfiguration of the intrinsic atoms reported here will prove to be a useful method for simply and widely tuning the lifetimes of light. Second, we observed asymmetric resonance profiles, which we occasionally call the Fano profiles, in the scattering cross-section spectra for the localized defect states created by the above method. These resonance profiles exhibited a variety of remarkable variations for their line shapes as a function of the incident direction of light. The present examination has made clear the correlations between the asymmetry of the spectra characterized by the so-called Fano's q value and the optical energy flows in the PC, in particular, that the optical incoming flux is maximized for $q^{-1} = 0$. This correlation is detected distinctly for the defect mode in the first gap, while it is observed in a certain frequency range for the defect modes in the second gap. The above fact demonstrates the presence of the selective photon capturing in the incoming processes of light and moreover, that it can be found out merely by the knowledge of the q value. This kind of approach will become an effective and convenient tool to clarify the intrinsic nature of the defect states introduced into the PCs: it suffices to measure the scattered-light intensity spectrum with high resolution. The present study may also be valid to evaluate the fluctuation of the lattice atoms in the regular PCs. We believe that this method will make a still more attractive tool for the analysis of the resonance states when it is extended to include a tomographic representation—what could be called *Fano Resonance Tomography*—that maps the q value for the differential scattering cross-section spectrum as a function of the scattering angle (θ_s) as well as the incident angle (θ_i).

[1] O. Painter, R. K. Lee, A. Scherer, A. Yariv, J. D. O'Brien, P. D. Dapkus, and I. Kim, Science **284**, 1819 (1999).

[2] *Optical Processes in Microcavities*, edited by R. K. Chang and A. J. Campillo (World Scientific, Singapore, 1996).

[3] *Cavity Quantum Electrodynamics*, edited by P. Berman (Academic Press, San Diego, CA, 1994).

[4] S. Nojima, Jpn. J. Appl. Phys. **37**, L565 (1998).

[5] S. Nojima, J. Appl. Phys. **90**, 545 (2001).

[6] S. Nojima, J. Appl. Phys. **98**, 043102 (2005).

[7] M. Meier, A. Dodabalapur, J. A. Rogers, R. E. Slusher, A. Mekis, A. Timko, C. A. Murray, R. Ruel, and O. Nalamasu, J. Appl. Phys. **86**, 3502 (1999).

[8] K. Inoue, M. Sasada, J. Kawamata, K. Sakoda, and J. W. Haus, Jpn. J. Appl. Phys. **38**, L157 (1999).

[9] C. Monat, C. Seassal, X. Letartre, P. Regreny, P. Rojo-Romeo, P. Viktorovitch, M. L. V. dYerville, D. Cassagne, J. P. Alber, E. Jalaguier, S. Pocas, and B. Aspar, Appl. Phys. Lett. **81**, 5102 (2002).

[10] S.-H. Kwon, H.-Y. Ryu, G.-H. Kim, Y.-H. Lee, and S.-B. Kim, Appl. Phys. Lett. **83**, 3870 (2003).

[11] S. Nojima, J. Phys. Soc. Jpn. **76**, 023401 (2007).

[12] S. Nojima and S. Nakahara, J. Appl. Phys. **109**, 093118 (2011).

[13] H.-B. Lin, J. D. Eversole, and A. J. Campillo, J. Opt. Soc. Am. B **9**, 43 (1992).

[14] B. Gayral, J. M. Gérard, A. Lemaître, C. Dupuis, L. Manin, and J. L. Pelouard, Appl. Phys. Lett. **75**, 1908 (1999).

[15] H.-J. Moon, Y.-T. Chough, and K. An, Phys. Rev. Lett. **85**, 3161 (2000).

[16] D. K. Armani, T. J. Kippenberg, S. M. Spillane, and K. J. Vahala, Nature (London) **421**, 925 (2003).

[17] C. Gmachl, F. Capasso, E. E. Narimanov, J. U. Nöckel, A. D. Stone, J. Faist, D. L. Sivco, and A. Y. Cho, Nature (London) **280**, 1556 (1998).

[18] J. Vučković, M. Lončar, H. Mabuchi, and A. Scherer, Phys. Rev. E **65**, 016608 (2001).

[19] H.-Y. Ryu, S.-H. Kim, H.-G. Park, J.-K. Hwang, Y.-H. Lee, and J.-S. Kim, Appl. Phys. Lett. **80**, 3883 (2002).

[20] T. D. Happ, I. I. Tartakovskii, V. D. Kulakovskii, J.-P. Reithmaier, M. Kamp, and A. Forchel, Phys. Rev. B **66**, 041303 (2002).

[21] Y. Akahane, T. Asano, B.-S. Song, and S. Noda, Nature (London) **425**, 944 (2003).

[22] S. John and J. Wang, Phys. Rev. B **43**, 12772 (1991).

[23] A. A. Maradudin and A. R. McGurn, in *Photonic Band Gaps and Localization*, edited by C. M. Soukoulis (Plenum Press, New York, 1993), p. 247.

[24] S. G. Johnson, S. Fan, A. Mekis, and J. D. Joannopoulos, Appl. Phys. Lett. **78**, 3388 (2001).

[25] J. Chaloupka, J. Zarbakhsh, and K. Hingerl, Phys. Rev. B **72**, 085122 (2005).

[26] N. Stefanou and A. Modinos, J. Phys.: Condens. Matter **3**, 8135 (1991).

[27] D. Felbacq, G. Tayeb, and D. Maystre, J. Opt. Soc. Am. A **11**, 2526 (1994).

[28] G. Tayeb and D. Maystre, J. Opt. Soc. Am. A **14**, 3323 (1997).

[29] S. Nojima and M. Nakahata, J. Appl. Phys. **106**, 043108 (2009).

[30] X.-P. Feng and Y. Arakawa, Jpn. J. Appl. Phys. **36**, L120 (1997).

[31] K. Amemiya and K. Ohtaka, J. Phys. Soc. Jpn. **72**, 1244 (2003).

[32] V. Kuzmiak and A. A. Maradudin, Phys. Rev. B **57**, 15242 (1998).

[33] K. Sakoda and H. Shiroma, Phys. Rev. B **56**, 4830 (1997).

[34] K. Sakoda, J. Appl. Phys. **84**, 1210 (1998).

[35] J. Vučković, M. Lončar, H. Mabuchi, and A. Scherer, Phys. Rev. E **65**, 016608 (2001).

[36] S. G. Johnson, S. Fan, A. Mekis, and J. D. Joannopoulos, Appl. Phys. Lett. **78**, 3388 (2001).

[37] T. Ueta, K. Ohtaka, N. Kawai, and K. Sakoda, J. Appl. Phys. **84**, 6299 (1998).

[38] J. Callaway, *Quantum Theory of the Solid State* (Academic Press, San Diego, CA, 1974).

[39] K. Ohtaka, in *Photonic Crystals*, edited by K. Inoue and K. Ohtaka (Springer, Berlin, 2004), p. 101.

[40] A. Temkin, *Autoionization: Recent Developments and Applications* (Kluwer Academic, Dordrecht, 1985).

[41] G. Herzberg, *Molecular Spectra and Molecular Structure: Spectra of Diatomic Molecules* (Krieger Publishing, Malabar, FL, 1989).

[42] N. F. Mott and H. S. W. Massey, *The Theory of Atomic Collisions* (Clarendon, 1987).

[43] U. Fano, Phys. Rev. **124**, 1866 (1961).

[44] A. E. Miroshnichenko, S. Flach, and Y. S. Kivshar, Rev. Mod. Phys. **82**, 2257 (2010).

[45] B. Luk'yanchuk, N. I. Zheludev, S. A. Maier, N. J. Halas, P. Nordlander, H. Giessen, and C. T. Chong, Nature Mater. **9**, 707 (2010).

[46] J. Faist, F. Capasso, C. Sirtori, K. W. West, and L. N. Pfeiffer, Nature (London) **390**, 589 (1997).

[47] H. Schmidt, K. L. Campman, A. C. Gossard, and A. Imamoğlu, Appl. Phys. Lett. **70**, 3457 (1997).

[48] S. Bar-Ad, P. Kner, M. V. Marquezini, S. Mukamel, and D. S. Chemla, Phys. Rev. Lett. **78**, 1363 (1997).

[49] K. Kobayashi, H. Aikawa, S. Katsumoto, and Y. Iye, Phys. Rev. Lett. **88**, 256806 (2002).

[50] H. C. Liu, C. Y. Song, Z. R. Wasilewski, J. A. Gupta, and M. Buchanan, Appl. Phys. Lett. **91**, 131121 (2007).

[51] G. Khitrova and H. M. Gibbs, Nature (London) **451**, 256 (2008).

[52] S. Fan and J. D. Joannopoulos, Phys. Rev. B **65**, 235112 (2002).

[53] V. Lousse and J. P. Vigneron, Phys. Rev. B **69**, 155106 (2004).

[54] T. Baba, H. Makino, T. Mori, T. Hanada, and T. Yao, Appl. Phys. Lett. **87**, 171106 (2005).

[55] F. Cheng, H. F. Liu, B. H. Li, J. Han, H. Xiao, X. F. Han, C. Z. Gu, and X. G. Qiu, Appl. Phys. Lett. **100**, 131110 (2012).

[56] M. V. Rybin, A. B. Khanikaev, M. Inoue, K. B. Samusev, M. J. Steel, G. Yushin, and M. F. Limonov, Phys. Rev. Lett. **103**, 023901 (2009).

[57] M. Galli, S. L. Portalupi, M. Belotti, L. C. Andreani, L. O'Faolain, and T. F. Krauss, Appl. Phys. Lett. **94**, 071101 (2009).

[58] S. Nojima and M. Yawata, J. Phys. Soc. Jpn. **79**, 043401 (2010).

[59] M. Abramowitz and I. A. Stegun, *Handbook of Mathematical Functions* (Dover, New York, 1972).

[60] L. D. Landau and E. M. Lifshitz, *Quantum Mechanics: Non-Relativistic Theory* (Butterworth-Heinemann, Oxford, 1981).

[61] E. Yablonovitch, T. J. Gmitter, R. D. Meade, A. M. Rappe, K. D. Brommer, and J. D. Joannopoulos, Phys. Rev. Lett. **67**, 3380 (1991).

[62] M. L. Ladrón de Guevara, F. Claro, and Pedro A. Orellana, Phys. Rev. B **67**, 195335 (2003).